Beach-face slope dataset for Australia

Kilian Vos[1], Wen Deng[1], Mitchell D. Harley[1], Ian L. Turner[1], Kristen D. Splinter[1]

[1]Water Research Laboratory, School of Civil and Environmental Engineering, UNSW Sydney, 110 King Street, Manly Vale, NSW 2093, Australia

5   *Correspondence to*: Kilian Vos (k.vos@unsw.edu.au)

Abstract. Sandy beaches are unique environments composed of unconsolidated sediments that are constantly reshaped by the action of waves, tides, currents, and winds. The most seaward region of the dry beach, referred to as the beach face, is the primary interface between land and ocean and is of fundamental importance to coastal processes, including the dissipation and reflection of wave energy at the coast, and the exchange of sediment between the land and sea. The slope of the beach-face is

10   a critical parameter in coastal geomorphology and coastal engineering, necessary to calculate the total elevation and excursion of wave run-up at the shoreline. However, datasets of the beach-face slope remain unavailable along most of the world's coastlines. This study presents a new dataset of beach-face slopes for the Australian coastline derived from a novel remote sensing technique. The dataset covers 13,200 km of sandy coast and provides an estimate of the beach-face slope at every 100 m alongshore, accompanied by an easy to apply measure of the confidence of each slope estimate. The dataset offers a unique

15   view of large-scale spatial variability in beach-face slope and addresses the growing need for this information to predict coastal hazards around Australia. The beach-face slope dataset and relevant metadata are available at https://doi.org/10.5281/zenodo.5606217 (Vos et al., 2021).

1 Introduction

The world's coastlines are unique geological environments at the interface between land and sea. Along this coastal fringe,

20   which is often densely populated (Small et al., 2011), we find beaches composed of unconsolidated sediments (e.g., gravel, sand, mud) that are constantly reshaped by the action of waves, currents, winds and tides (Dean and Dalrymple, 2004). A typical beach cross-section, or beach profile, is illustrated in Figure 1. The beach face is the most seaward region of the subaerial beach, which extends from the berm to the low tide water line and is constantly interacting with the uprush and downrush of individual waves and tidal cycles. The steepness of the beach face (tanβ), or beach-face slope, is a key parameter

25   in coastal geomorphology and coastal engineering due to its control on important coastal processes. Crucially, the beach-face slope controls the elevation of wave run-up and total swash excursion at the shoreline (Gomes da Silva et al., 2020; Stockdon et al., 2006), processes that are of primary importance for the assessment of coastal erosion and inundation hazards along the coastal boundary (Senechal et al., 2011; Stockdon et al., 2007). The beach-face slope parameter is also a useful proxy for surf-zone hydrodynamics in the absence of costly surf-zone bathymetric surveys and can provide insights into beach swimmer

30   safety (Short et al., 1993) and wave set-up across the surf zone (Stephens et al., 2011).

Despite the importance of the beach-face slope parameter in numerous empirical formulations in coastal engineering (e.g., wave run-up prediction), large-scale datasets of the beach-face slope remain unavailable along most of the world's coastlines. A complementary global dataset of nearshore slopes, defined from Mean Sea Level (MSL) to the 'closure depth' where negligible morphological change theoretically occurs, was recently compiled by Athanasiou et al. (2019). Referring to Figure 1, this slope indicates the cross-shore gradient of the subaqueous (below MSL) profile and is generally much lower in gradient than the beach-face slope.

The steepness of the beach face is closely related to grain size (Bujan et al., 2019), with coarser/finer sediment typically adopting a steeper/flatter beach face, however it is also linked to the morphodynamic beach state, with lower-gradient slopes usually found along high-energy dissipative beaches and steeper slopes along low-energy reflective beaches (Wright and Short, 1984). The beach-face slope can be measured by using survey techniques such as topographic RTK-GPS measurements, but these methods require human intervention and remain impractical over large spatial scales (regional to continental). In recent decades, Airborne LiDAR technology has significantly increased the spatial coverage of coastal topographic data, from individual beaches to hundreds of kilometres of coastline (e.g., Middleton et al., 2013; Stockdon et al., 2002). However, in the swash zone, these active remote sensing techniques are hampered by the constant alternating of wet and dry phases as water levels fluctuate at the shoreline under the action of waves and tides slopes (Middleton et al., 2013), limiting the ability to extract beach-face slopes. UAV surveys and aerial photogrammetry are also subject to the same caveat as structure-from-motion techniques fail in the swash zone due to the non-stationary ground target (Pucino et al., 2021; Turner et al., 2016). More recently, novel methods to extract intertidal zone information using publicly available optical imagery and tide models have been developed (Bishop-Taylor et al., 2019; Tseng et al., 2017), considerably increasing our ability to map coastal topography over large spatial scales. In particular, Vos et al. (2020) introduced a method to specifically estimate the beach-face slope combining instantaneous satellite-derived shorelines with predicted tides and capable of accurately estimating the long-term average slope between MSL and Mean High Water Springs (MHWS), the region highlighted in Figure 1, across a wide range of coastal environments. This new method paves the way for the generation of large-scale beach-face slope datasets to complement the present nearshore slope global dataset and better resolve the coastal topography.

In Australia, a national dataset of coastal topography and bathymetry was recently identified by the marine research, industry and stakeholder communities as the highest ranked priority for wind-waves research (Greenslade et al., 2020). It is noted in this report that a coastal elevation dataset will significantly improve *"our ability to model other hazards such as tsunamis and storm surges, as well as providing information to improve marine management including marine planning, monitoring, research, and emergency response"*. In a similar study Power et al. (2021) also identified data collection from remotely sensed products (referred to as item DAT3) as one of the key research priorities in coastal geosciences. More specifically, O'Grady et al. (2019) investigated the contribution of wind waves to total water levels along the Australian coastline and concluded that a key limitation for an accurate Operational Coastal Inundation Forecasting System is the lack of a continental-scale beach-face slope dataset. Historically, due to there being no alternative, studies that have focused on continental to

regional scales have adopted uniform beach-face slope values. For example, recent studies investigating the contribution of

65   wave processes to relative sea-level-rise have either used slope-independent runup formulations (Vitousek et al., 2017) or

opted for a constant and therefore arbitrary beach-face slope of 0.1 for all of the world's coastlines (Melet et al., 2018) which

has attracted criticism of this approach (Aucan et al., 2019).

In this contribution, we use a recently published and validated beach slope estimation technique (Vos et al., 2020) to fill this

gap for the Australian continent. We present a new dataset of beach-face slopes spaced at 100 m increments alongshore for

70   every sandy beach in Australia totalling 13,200 km of sandy coastline. Each beach-face slope estimate is based on the average

slope over the past 20 years and is associated with an easy-to-apply measure of confidence. The methodology to estimate

beach-face slopes and confidence bands is presented in the next section. A synopsis then follows of the large-scale spatial

variability in beach-face slopes around the Australian continent, and the integration of this dataset with the National Sediment

Compartment Framework for Australia (Thom et al., 2018). The paper concludes with a brief section illustrating potential use

75   cases of this new dataset for coastal management and inundation forecasting studies.
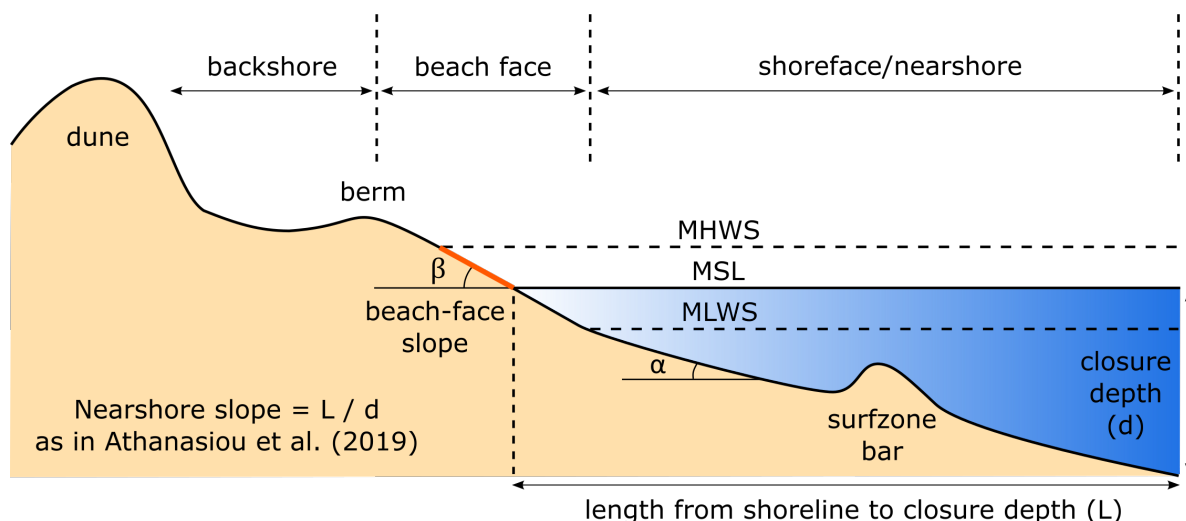
Figure 1. Schematic of a beach profile from the dune to the depth of closure, adapted from Coastal Engineering Research Center (1984). The beach-face slope (tanβ) that is mapped in this work is a proxy for the slope of the portion of the profile that is highlighted in orange, extending from Mean Sea Level (MSL) up to Mean High Water Spring (MHWS). The beach-face slope complements the global dataset of nearshore slopes presented in Athanasiou et al. (2019) that represents the slope extending from the depth of closure up to MSL.

2 Methods

2.1 Transects dataset

A dataset of shore-normal transects along the Australian sandy coastline was created semi-automatically. Sandy beaches were

first extracted from the OpenStreetMaps database (OSM, 2017) and manually quality-controlled in a GIS environment (QGIS

85   Development Team, 2021). In total, 5,207 sandy beaches were identified along open coasts and semi-enclosed regions. The

sandy shoreline locations were then used to generate 100 m alongshore-spaced cross-shore transects with the "*v_transects*"
functionality of GRASS GIS (GRASS Development Team, 2020), generating a total of 132,000 individual transects extending
along 13,200 km of sandy coastline circumnavigating the Australian continent. The beach-face slope was estimated along
each transect as described in the following section.

90 **2.2 Beach slope estimation algorithm**

A novel remote sensing technique to estimate beach-face slopes from satellite imagery and modelled tides was applied to each
of the 132,000 sandy beach transects. This method is described in detail in Vos et al. (2020) and combines 20-year time-series
of shoreline change derived from Landsat imagery with tidal predictions at the time of image acquisition to estimate the slope
of the beach face. Briefly, the concept behind this method is that instantaneous shoreline time-series, mapped on images that
95 were acquired at different stages of the tide, contain a tidal signal that is modulated by the beach-face slope and can be isolated
in the frequency domain due to its periodicity. Thus, this technique uses the frequency domain and iteratively seeks a value of
the slope that minimises the tidal energy when used for tidal correction. Tidal correction consists of the projection of individual
instantaneous shorelines, acquired at different stages of the tide, to a standard reference elevation such as MSL. A simple tidal
correction is then applied by translating horizontally the shoreline points along a cross-shore transect using a linear slope:

100
$$\Delta x_{corrected} = \Delta x + \frac{z_{tide}}{tan\beta} \qquad (1)$$

where $\Delta x_{corrected}$ is the tidally-corrected cross-shore position, Δx is the instantaneous cross-shore position, z_{tide} is the
corresponding tide level and tanβ is the beach-face slope.

The first step is to map instantaneous shorelines spanning a full 20 years of all available Landsat imagery (Landsat 5, 7 and
105 8) at every sandy beach and then determine the intersection of individual shorelines with each of the 100 m spaced transects
to obtain time-series of (non-tidally corrected) shoreline change, an example of this is shown in Figure 2a for Cable Beach,
Western Australia. The time-series were obtained with the open-source CoastSat toolbox — publicly available at
https://github.com/kvos/CoastSat and described in Vos et al., (2019). Next, tide levels associated with every shoreline
observation are extracted from the global tide model FES2014 (Carrere et al., 2016), as shown in Figure 2b. The tide level
110 time-series are then transformed to frequency domain, and since these are not evenly sampled (as shorelines are not mapped
on all the images because of cloud cover, false detections and other issues), a variant of the Fourier transform, the Lomb-
Scargle transform (VanderPlas, 2018) is employed to compute the power spectrum density (PSD). The frequency with the
highest peak is then isolated from the PSD, which corresponds to the frequency where the tidal signal (e.g. the spring-neap
tidal cycle) is the strongest in the sub-sampled time-series, referred to as the 'peak tidal frequency'. The final step to obtain
115 the time-averaged estimated beach-face slope at every 100 m alongshore location consists of tidally-correcting the time-series

of uncorrected shoreline change using an iterative range of slope values from 0.01 to 0.2 (from Bujan et al., (2019)), transforming each tidally-corrected time-series to frequency domain and integrating each PSD inside the peak tidal frequency band to construct a curve of tidal energy vs slope (Figure 2c). The best estimate of the beach slope is then the value that minimises this tidal energy in the peak tidal frequency band (Figure 2d).

120   This beach-face slope estimation technique was validated against *in situ* (beach survey) data along 8 diverse sandy/gravel beaches spanning a broad range of beach-face slopes, tidal regimes, and wave climates (Vos et al., 2020). The validation sites — namely Narrabeen-Collaroy, Moruya-Pedro and Cable Beach in Australia, Duck and Torrey Pines in the USA, Slapton Sands UK, Tairua Beach NZ, and Ensenada MEX — range from microtidal wave-dominated to macrotidal tide-modified beaches, with the *in situ* measured average beach-face slopes varying from $\tan\beta = 0.025$ to $\tan\beta = 0.14$. A strong correlation

125   (R^2 of 0.93) was found between *in situ* and satellite-derived beach-face slope estimates, with no systematic under- or over-estimation observed, demonstrating the applicability of this method across a wide range of coastal environments.
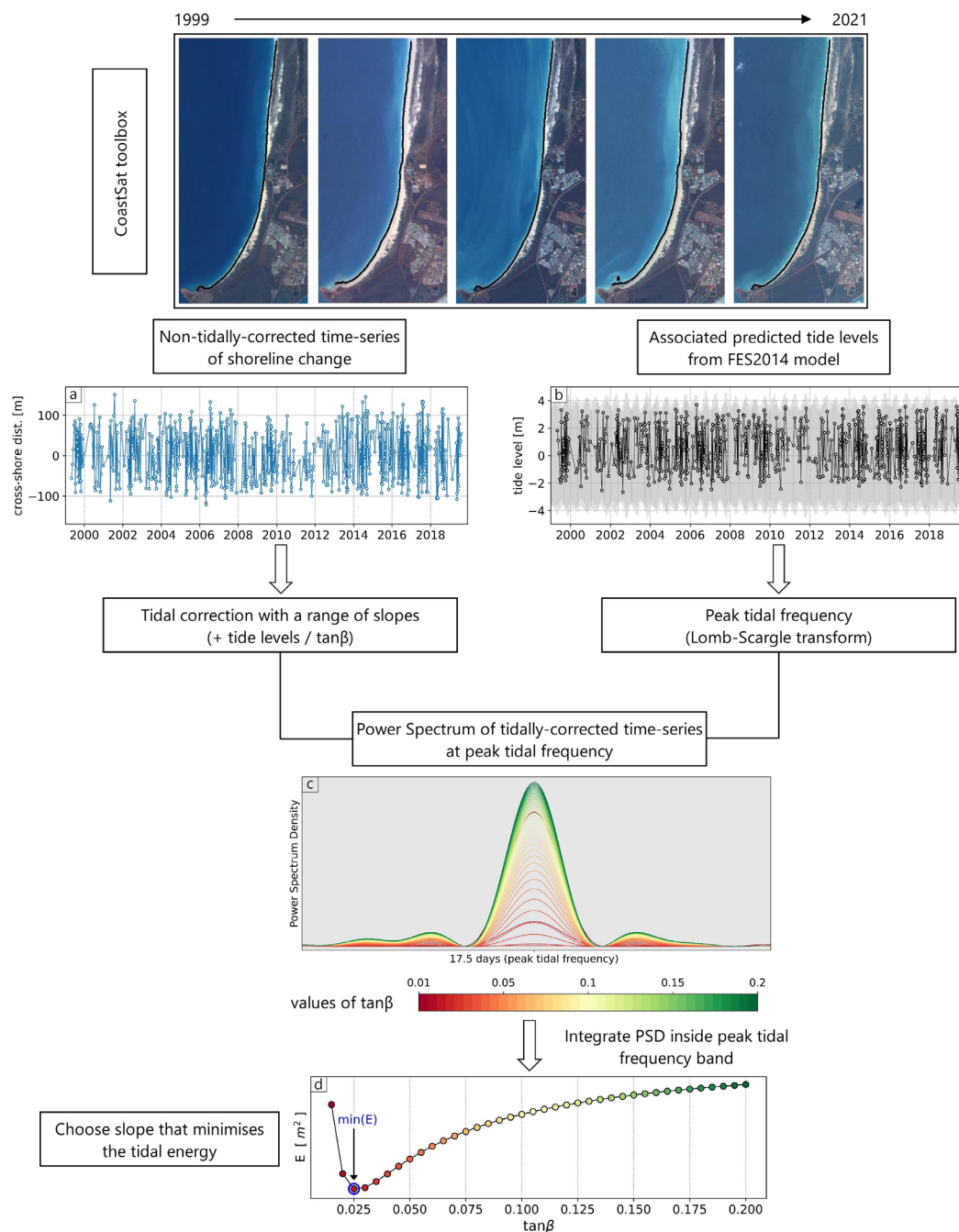
Figure 2. Flowchart of the methodology to estimate beach-face slopes from satellite-derived shorelines and predicted tides described in Vos et al. (2020). Firstly, instantaneous shorelines are mapped on Landsat imagery with the CoastSat toolbox. The time-series of non-tidally corrected shoreline change (a) and their associated tide levels (b) are then combined in frequency domain to find the slope that, when used for tidal correction, minimises the tidal signal. (c) shows the power spectrum density (PSD) of the tidally-corrected time-series, demonstrating how the slope value modulates the energy inside the tidal frequency band, plotted as a function of slope in (d).

130

Earth System
Science
Data

Open Access

Discussions

2.3 Beach-face slope confidence bands

The tidal energy vs beach-face slope curve shown in Figure 2d is used to quantify the uncertainty of each beach-face slope
135   estimate. When the minimum is very well defined in the curve (as in Figure 2d), this indicates high confidence in the estimate
as there is a single value of the slope that clearly minimises the amount of energy in the peak tidal frequency band. However,
at other locations, the minimum of the curve is not so well defined, and several beach-face slope values correspond to similar
levels of PSD energy, as shown in Figure 3 (from Narrabeen-Collaroy beach located in Sydney, NSW). To incorporate a
simple-to-apply measure of uncertainty in the dataset of beach-face slope estimates, a 5% vertical band above the minimum
140   amount of energy in the curve is used to estimate confidence bands around the slope estimate. To illustrate, Figure 3 shows
the 5% band above the minimum energy, the slope that minimises the energy (0.075), and the lower bound (0.065) and upper
bound (0.095) slopes that define the 5% of the minimum PSD energy. Note that given the shape of the energy vs beach-face
slope curves, which generally tends to start as a parabola and then flatten with an inflection point after the minimum, the
confidence bands are not symmetric.
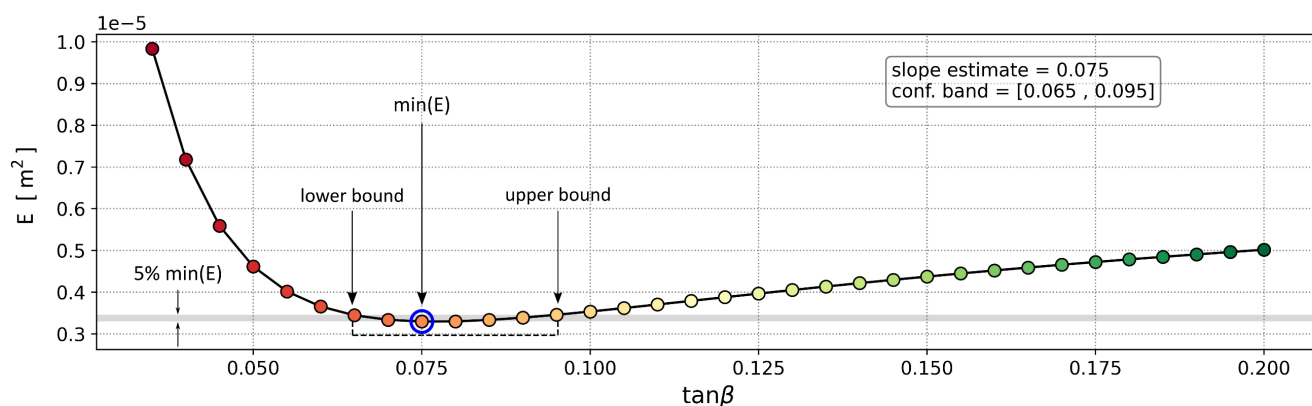
Figure 3. Estimation of confidence bands around each beach-face slope estimate based on the tidal energy vs slope curve. The lower and upper bounds are the slopes that are associated with a tidal energy within 5% of the minimum.

3 Results

3.1 Synopsis of the distribution of beach-face slopes around Australia

150   Beach-face slopes were estimated at each of the 132,000 beach transects, corresponding to 13,200 km of sandy coastline
around Australia. The beach slope data was summarised from the transect scale to the individual beach scale by calculating
the weighted average of all the transects at each beach, weighted by the width of the confidence bands to emphasise slopes
with higher confidence. The resulting average beach-face slope for every sandy beach around the continent is presented in
Figure 4a. Beach-face slope values range between 0.01 and 0.18. The distribution of beach-face slopes for each of the 7 coastal

155 states in Australia is shown in Figure 4b, indicating median values between 0.055 (Victoria) and 0.08 (Northern Territory), with all 7 interquartile ranges sitting between 0.045 and 0.11.

Along the wave-dominated and energetic southern half of Australia (refer Supplementary Figure 1b), the dataset shows very low gradient beaches (0.01-0.035) along the western coast of Tasmania, western Victoria, and south-west WA. Large spatial variability in beach-face slopes is observed along the tide-modified/tide-dominated northern half of Australia, with

160 Queensland showing the widest interquartile range (from 0.05 to 0.11).
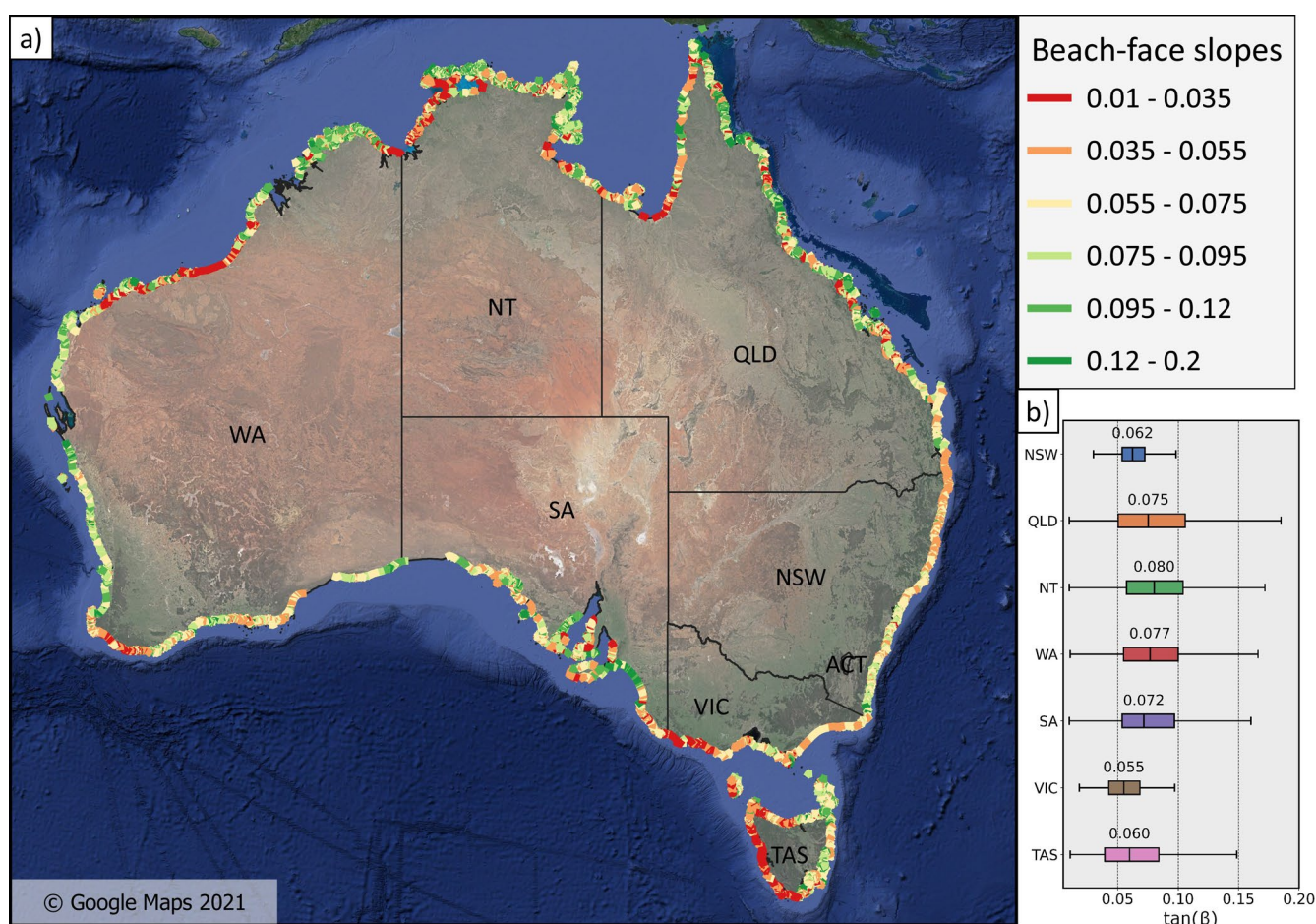
Figure 4. Beach-face slopes around Australia along 132,000 100m-spaced transects (equivalent to 13,200 km of coast). (b) shows the distribution for each Australian state.

While State administrative boundaries provide a first division of the country, useful for high-level management purposes, they

165 are not representative of the geology, surface landforms and shoreline orientation of the Australian coastline. To address this, Thom et al. (2018) proposed a national sediment compartment framework that provides a hierarchical division of the coast integrating inshore/offshore geological factors, major structural landforms such as headlands and changes in shoreline orientation. On this basis, the Australian continent is divided into 23 coastal 'regions', 100 'primary sediment compartments'

and 361 'secondary sediment compartments'. The beach-face slope distribution (weighted-average per beach) for each of the
23 coastal regions is presented in Figure 5. Along the south-eastern coast, narrow slope distributions are observed in Central
East (2), Southern NSW (1) and Gippsland (20). Moving northwards, very wide distributions are observed in Central
Queensland (3), Eastern (4) and Western Cape York Peninsula (5), and Southern Gulf of Carpentaria (6). The Northern
Territory (NT) shows a clear contrast between the relatively steep beaches of East and North Arnhem Land (7-8) and the
extremely low gradient Western NT (9). A similar distinction is observed in the northern part of Western Australia (WA),
where the manifold of islands in the Kimberley region (10) show steep slopes that contrast with the long and low gradient
beaches of the Pilbara region (11). As the tide-modified/tide-dominated coast transitions to wave-dominated, a gradient of
decreasing beach slopes is observed along the western regions of Central West WA (12), Southwest WA (13) and Southern
WA (14). Wide beach-face slope distributions are observed in South Australia (SA), regions 15-18, which comprises long
microtidal coasts, mesotidal gulfs and large offshore islands. The remaining region of the continental mainland is Central and
Western Victoria (19), which contains relatively low gradient beaches (median of 0.05). Finally, in Tasmania a clear distinction
between the intermediate slopes of the North (21) and East coasts (22) and the West (23) coast is apparent, noting that West
Tasmania exhibits the lowest beach-face slopes (median 0.03) of all the coastal regions around Australia.
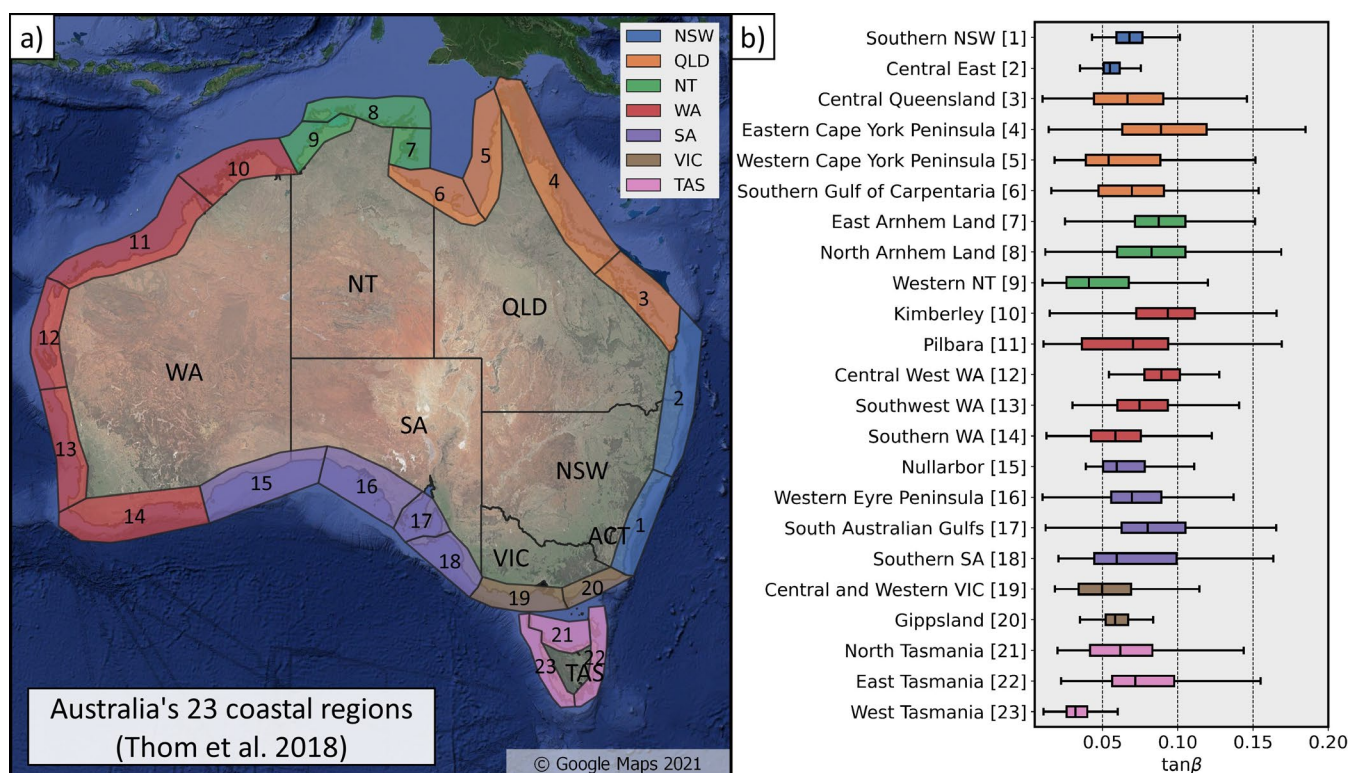
Figure 5. Distribution of beach-face slopes for each of the 23 coastal regions identified by Thom et al. (2018).

185   The widths of the corresponding beach-face slope confidence bands, described in Section 2.3 provide a simple-to-apply metric and filter on the uncertainty in slope estimates. Figure 6a presents a map of the beach-averaged width of the confidence bands, color-coded with a simple three-category 'traffic-light' system: *high confidence* (green) when below 0.025, *medium confidence* (yellow) between 0.025 and 0.05 and *low confidence* (red) above 0.05. Using these categories, 56% of the continental-scale dataset indicate *high confidence*, with 23% *medium confidence* and 21% *low confidence*. Figure 6b shows the distribution of

190   this confidence metric across each of the 23 regions. Extensive areas of low confidence are observed along the west and south coasts of WA and most of SA, while the remainder of the coastline generally indicates high confidence, interspersed by isolated occurrences of low/medium confidence (e.g., east Arnhem Land, south-east Tasmania). The median width of confidence bands is below 0.025 (i.e., high confidence) for 13 of the 23 coastal regions, between 0.025 and 0.5 (medium confidence) for 5 regions (East Arnhem Land, Central West WA, Western Eyre Peninsula, East/West Tasmania) and above

195   0.5 (low confidence) for 5 regions including south-west and southern WA and the majority of SA.
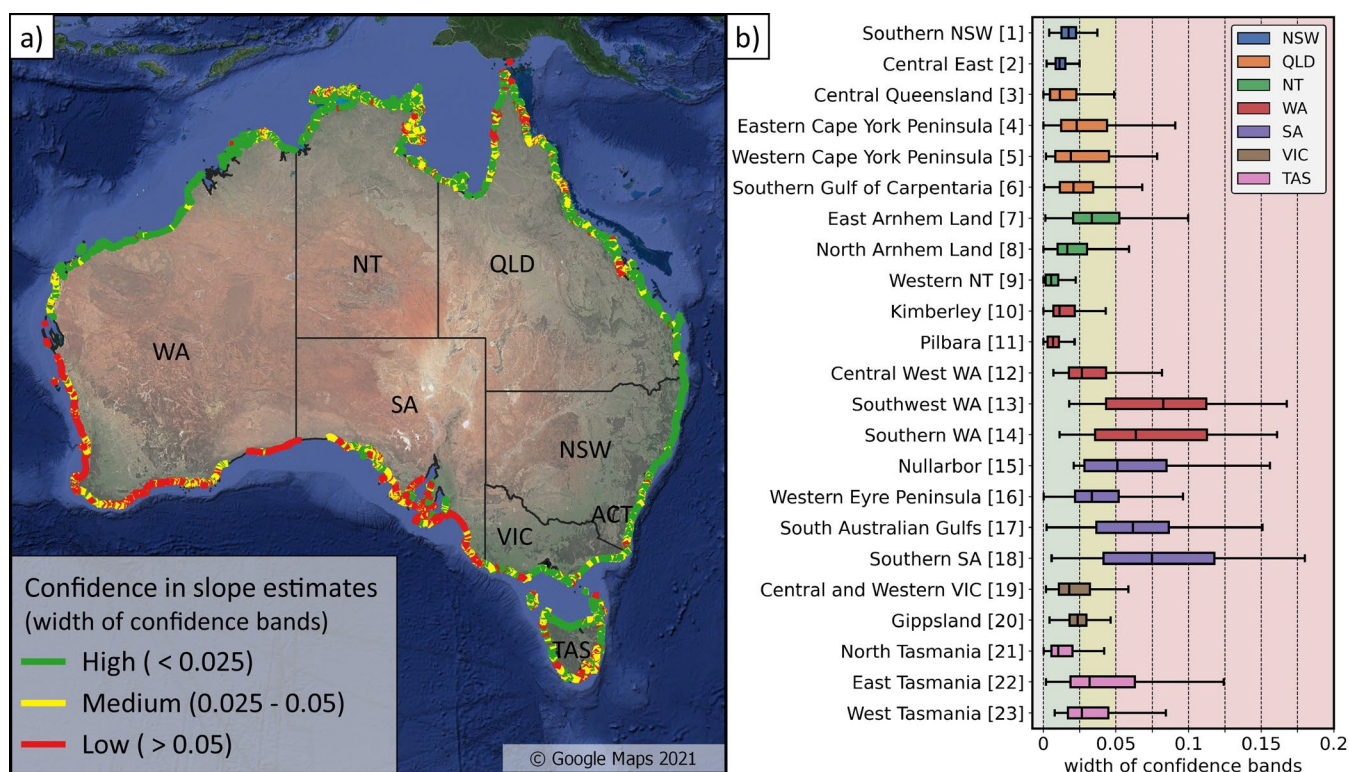

Figure 6. Traffic-light system indicating the uncertainty in the beach-face slope estimates. (b) shows the distribution of the width of confidence bands across the 23 regions, indicating on average high confidence across 13 regions, medium confidence across 5 regions (7,12,16,22,23) and low confidence across 5 regions (13,14,15,17,18).

200   Vos et al. (2020) previously identified that the performance of the beach slope estimation method depends on the signal-to-noise ratio between the accuracy of the satellite-derived shorelines (10-15m based on the validation in Vos et al. (2019b)) and

the horizontal extent of the tidal excursion. Thus, the observation of greater uncertainty in slope estimates along south-west and south WA regions is consistent with the very small tidal range along this coast (< 1 m Mean Spring Tidal Range, see Supplementary Figure 1a). Another issue affecting the signal-to-noise ratio is the aliasing of the tidal signal by sun-

205 synchronous sensors (i.e., Landsat orbits), which means that the full tidal range may not always be captured by the satellite imagery (Bishop-Taylor et al., 2019; Eleveld et al., 2014). Figure 7 shows the percentage of the Mean Spring Tidal Range (MSTR) that is observed by the satellite-derived shorelines at each beach. This analysis reveals that the SA coastal regions (15-18), which exhibit lower confidence in Figure 6, have the lowest tide range coverage with only about 60-65% of the MSTR sampled (Figure 7a). Thus, along the SA regions which are already microtidal (except inside the gulfs), this aliasing

210 results in only part of the tidal range being observed in the available satellite imagery, further reducing the signal-to-noise ratio and leading to lower confidence slope estimates.
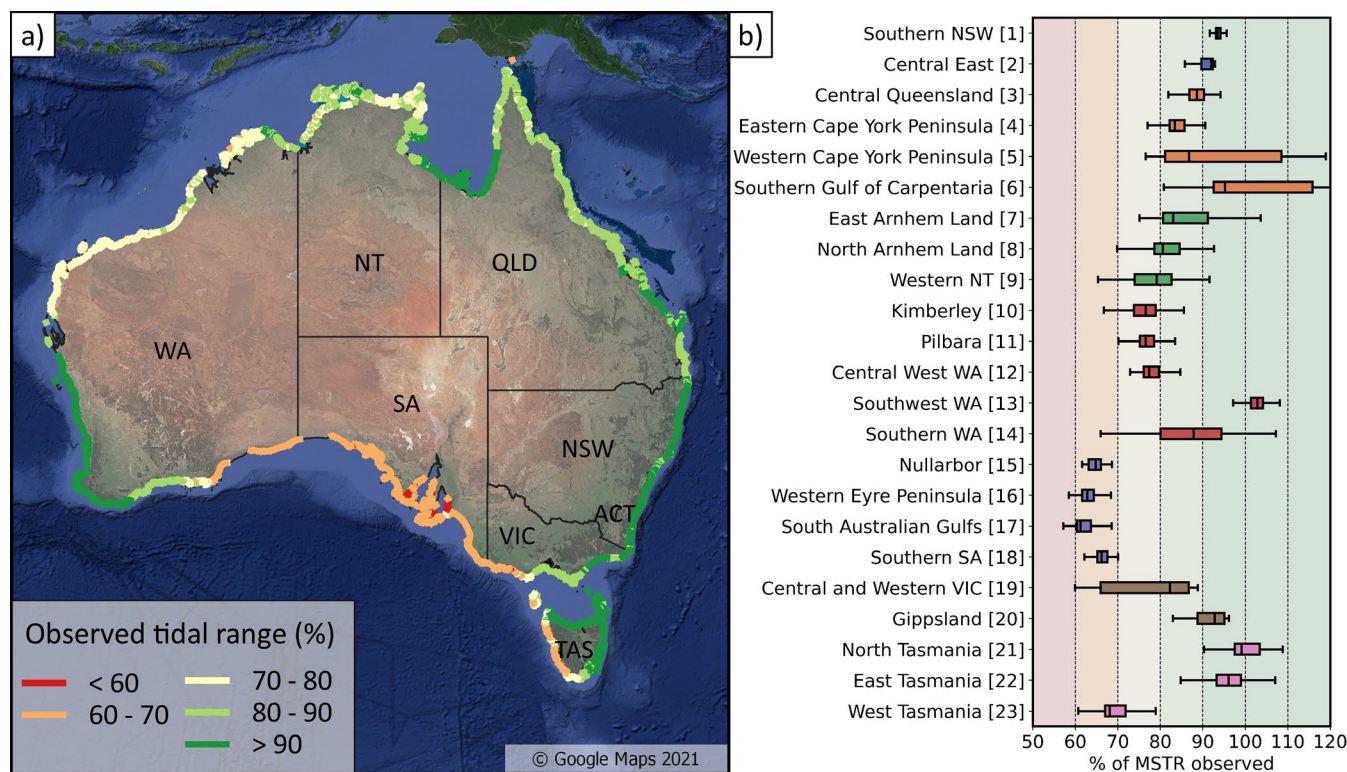

Figure 7. Observed tidal range by the satellite-derived shorelines. (a) maps the % of the MSTR that is observed at each beach and (b) shows the distribution of that metric across the 23 coastal regions.

215 **3.2 An example embayment-scale application**

While the previous section focused on the large-scale distribution of beach-face slopes at the continental scale, this dataset can also provide insights into variations in beach-face slope along any individual embayment or beach. To illustrate, Figure

8a shows beach-face slopes at the transect-scale (100 m spacing alongshore) along a single embayment, the Stockton Bight, located in NSW about 150 km north of Sydney. Stockton Bight is the longest beach in NSW, featuring 32-km of south-facing

220   sandy coast backed by a large transgressive dune system (Short, 2020). The beach-face slope data at this site, shown in Figure 8a, indicates a distinct alongshore gradient, with lower gradient slopes towards the northern end of the embayment ($\tan\beta$ = 0.04) and steeper slopes in the southern ($\tan\beta$ = 0.1). Interestingly, a sediment grain size dataset at this same site is reported by Pucino (2015), with the median swash zone sand size (D_{50}) at 20 equally spaced sample locations (Figure 8b) indicating a distinct gradient in grain size along the Stockton Bight embayment. The observed correlation between grain size and beach-

225   face slope that is apparent in Figure 8 is in agreement with our understanding of this relationship, generally described by a power-law (Bujan et al., 2019). This example demonstrates that this continental-wide dataset can also be utilised to gain insights into the alongshore variability of beach-face slopes (and, potentially, grain size distribution) along individual beaches and embayments, and inform present-day coastal management and planning.
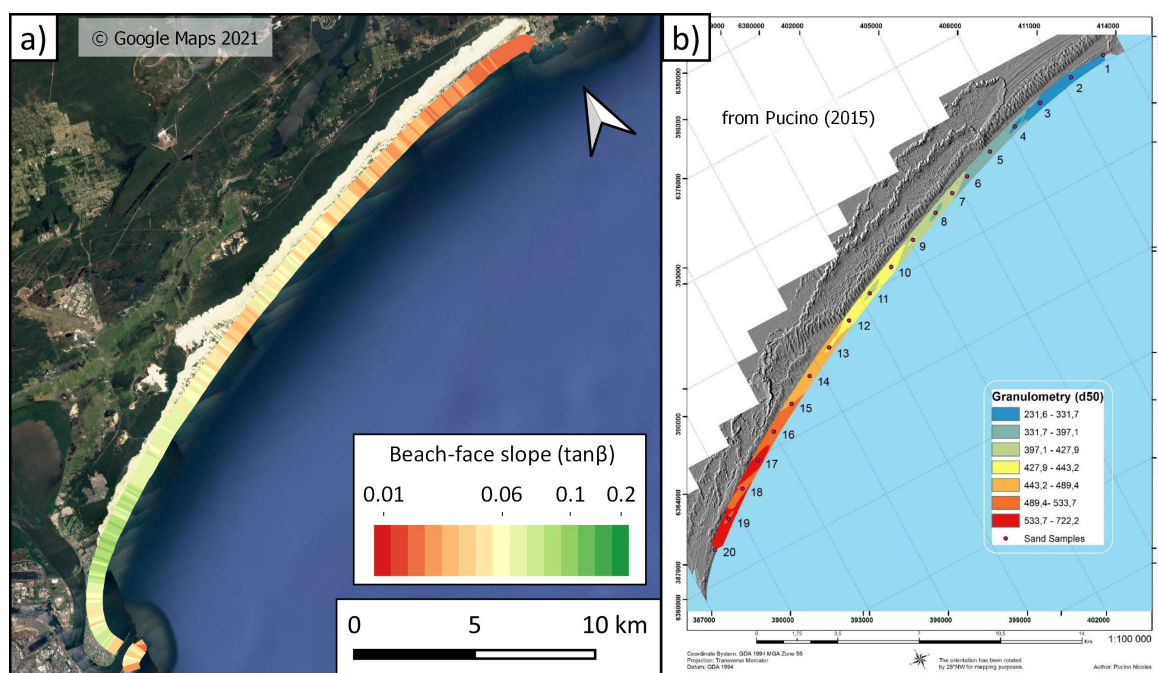
230   **Figure 8.** Embayment-scale gradient in beach-face slopes and sediment grain size. a) Beach-face slope estimates along 100-m spaced cross-shore transects along the Stockton Bight embayment. b) Figure taken from Pucino (2015) displaying the spatial distribution of median grain size (D_{50}) for 20 sand samples along the embayment. D_{50} values are in microns and have been interpolated using inverse-weighted-distance and discretised into 7 quantiles.

3.3 Dataset description

235 The data presented above is made available as two geospatial layers (GeoJSON files): one providing the beach slope estimates on a transect basis (100 m alongshore spacing) and the second providing the estimates averaged over each individual beach. Tables 1 and 2 describe the attributes of each layer, respectively.

At the transect scale (Table 1), the beach-face slope and confidence bands are accompanied by relevant metadata such as the number of shoreline points used to estimate the beach slope, the sediment compartment/region in which the transect is located

240 and a database id for the transect. A confidence flag (high/medium/low) is associated with each estimate as is illustrated in Figure 6.

At the beach scale (Table 2), the alongshore-averaged slope weighted by the width of the confidence intervals is provided for each individual beach, associated with a confidence flag (high/medium/low) based on the alongshore-averaged width of the confidence bands. Relevant metadata at the beach scale include the Mean Spring Tide Range (MSTR), Median Significant

245 Wave Height (Hsig), Percentage of Observed Tide Range and beach length.

To assist users of Australia's national sediment compartment framework (Figure 5), the distribution of beach slopes in each sediment compartment is provided in Supplementary Information at both the primary (Supplementary Figure 3) and secondary (Supplementary Figure 4) levels. Geospatial layers containing the primary and secondary compartments are also included in the dataset and displayed in Supplementary Figure 2.

250

Table 1. Description of data fields for the beach-face slope dataset at the transect scale

Attributes	Values	Description
Transect id	e.g., aus0001-0000, aus0001-0001, …	Database id for each transect
Beach id	e.g., aus0001, aus0002, …, aus5255	Database id for each beach
Beach-face slope ($tan\beta$)	value between 0.01 and 0.2	Estimate of the beach-face slope (between MSL and MHWS)
Lower confidence bound	value between 0.01 and 0.2	Lower limit of the confidence band
Upper confidence bound	value between 0.01 and 0.2	Upper limit of the confidence band
Width of confidence band	value between 0 and 0.19	Width of confidence band
Number of shoreline points	value between 100 and 1300	Number of datapoints in the time-series used for beach-face slope estimation.
Confidence flag	High/Medium/Low confidence	Quality flag indicating the confidence in the slope estimate at this transect

Coastal region	e.g., Southern NSW, Central Queensland, …	Database id corresponding to the 23 coastal regions as identified by Thom et al. (2018)
Primary Sediment Compartment	e.g., NSW01.01, NSW01.02, QLD01.01, …	Database id corresponding to the 100 primary sediment compartments as identified by Thom et al. (2018)
Secondary Sediment Compartment	e.g., NSW01.01.01, NSW01.01.02, QLD01.01.01, QLD01.01.02, …	Database id corresponding to the 361 secondary sediment Compartments as identified by Thom et al. (2018)

Table 2. Description of data fields for the beach-face slope dataset at the individual beach scale

Attributes	Values	Description
Beach id	e.g., aus0001, aus0002, …, aus5255	Database id for each beach
Average beach-face slope $(\overline{tan\beta})$	value between 0.01 and 0.2	Average of the beach-face slope along each transect, weighted by the width of the confidence bands
Average width of confidence bands	value between 0 and 0.19	Average width of confidence band over the comprised transects
Average number of shoreline points	value between 100 and 1300	Average number of datapoints in the time-series over the comprised transects
Confidence flag	High/Medium/Low confidence	Quality flag indicating the confidence in the slope estimate at this beach
Coastal region	e.g., Southern NSW, Central Queensland, …	Database id corresponding to the 23 coastal regions as identified by Thom et al. (2018)
Primary Sediment Compartment	e.g., NSW01.01, NSW01.02, QLD01.01, …	Database id corresponding to the 100 primary sediment compartments as identified by Thom et al. (2018)
Secondary Sediment Compartment	e.g., NSW01.01.01, NSW01.01.02, QLD01.01.01, QLD01.01.02, …	Database id corresponding to the 361 secondary sediment Compartments as identified by Thom et al. (2018)

Mean Spring Tide Range (MSTR)	value between 0.75 m and 10 m	Mean Spring Tide Range at the beach calculated from the closest grid point in the FES2014 global tide model (Carrere et al., 2016)
Median Significant Wave Height (Hsig)	value between 0.1 m and 3 m	Median Significant Wave Height from the closest grid point in the CAWCR re-analysis dataset
Percentage of MSTR observed	value between 57% and 130%	Percentage of the MSTR observed by the satellite-derived shorelines as: $100 \dfrac{\max(tide_{observed}) - \min(tide_{observed})}{MSTR}$
Beach length	value between 75 m and 50 km	Length of each beach or embayment. Very long beaches (> 50 km) were split to optimise memory as images are cropped around each beach

5 Conclusion and Outlook

255   This study presents a new dataset of beach-face slopes for the Australian coastline derived from a newly-available remote sensing technique. The dataset covers a total of 13,200 km of sandy coast and provides an estimate of the beach-face slope from Mean Sea Level (MSL) to Mean High Water Spring (MHWS) spaced every 100 m alongshore. The beach-face slope estimates are obtained from satellite observations spanning the past two decades and represent the long-term average beach-face slope, and therefore do not capture potential temporal variability. The slope estimation method is based on the value of

260   the slope that minimises the tidal energy when used to tidally-correct satellite-derived shoreline time-series and has been validated (Vos et al., 2020) across a diverse range of coastal environments. Each slope estimate is accompanied by confidence bands that indicate the upper and lower slope limits that would account for a modulation of the tidal energy within 5% of the minimum. While these are not 95% confidence intervals in the statistical sense, they provide practical information for end-users about the uncertainty associated with any individual slope estimate. Based on the width of the confidence bands. 56%

265   of the continental-scale dataset are classified *high confidence*, with 23% indicating *mediun confidence* and 21% *low confidence*. Regions of relatively low confidence are predominantly located along the south and south-western coasts. Vos et al. (2020) demonstrated that the accuracy of this method is linked to the signal-to-noise ratio of the satellite-derived shorelines relative to the tidal excursion signal (dependent on the tidal range and the slope itself). Here we show that these low-confidence areas are characterised by the smallest tidal range in the country (MSTR < 1m) in the case of the south-western sector, while

270 along the South Australia regions only part of the full tidal range (60-70%) is observed by the sun-synchronous satellite sensors as a result of an aliasing effect (Bishop-Taylor et al., 2019; Eleveld et al., 2014).

This new dataset provides critical information for the better understanding of coastal processes around Australia and complements an existing dataset of nearshore slopes measured between MSL and the depth of closure provided by Athanasiou et al. (2019). While the nearshore slopes can be used to transform offshore wave parameters to the nearshore (see Figure 1),

275 the beach-face slope is necessary to predict the elevation of wave run-up and total swash excursion at the shoreline. For this reason, the beach-face slope dataset is important for improving predictions of coastal erosion and inundation along the Australian coast (O'Grady et al., 2019) and assessing coastal inundation hazards and potential damage to beach-front infrastructure. Furthermore, in the context of an operational coastal flood warning system for sandy beaches (e.g., Leaman et al., 2021; Stokes et al., 2019) the confidence bands associated with each slope estimate are key to propagate the uncertainty

280 into the run-up equations and provide equivalent confidence bands for the total run-up elevation and swash excursion predictions.

In conclusion, this new dataset offers a unique view of large- to local-scale scale features in beach-face slope variability, providing data in regions with no *in situ* observational coverage. The new dataset can be exploited i) to better understand large-scale geologic factors contributing to the distribution of beach-face slopes and sediment grain size (Bujan et al., 2019;

285 Short, 2020), ii) to inform coastal management and coastal planning at the embayment scale (e.g., Figure 8), including tourist perception of the beach (Phillips and House, 2009) and beach-front property value (Gopalakrishnan et al., 2011), iii) to improve run-up predictions for an operational coastal inundation forecasting system (O'Grady et al., 2019), iv) to supplement and enhance assessments of beach swimmer safety and surf hazard like the Australian Beach Safety and Management Program (Short et al., 1993).

290 **Data Availability**

The continental-scale beach-face slope dataset described in this manuscript (Section 3.3) is available in the following Zenodo data repository: https://doi.org/10.5281/zenodo.5606217 (Vos et al., 2021).

Code Availability

The source code to map satellite-derived shorelines from Landsat imagery (CoastSat) is available at

295 https://doi.org/10.5281/zenodo.2779293 (Vos, 2021a). The source code to estimate beach slopes from satellite-derived shorelines and modelled tides (CoastSat.slope) is available at https://doi.org/10.5281/zenodo.3872442 (Vos, 2021b).

Earth System
Science
Data

Open Access   Discussions

305   **Author Contribution**

K.V., W.D., M.H.D., I.L.T. and K.D.S. devised the study, designed the figures, and wrote the manuscript. W.D. prepared the transect dataset and K.V. processed the beach-face slope data. All authors discussed the results and reviewed the manuscript.

Competing Interest

The authors declare that they have no conflict of interest.

310   **References**

Athanasiou, P., van Dongeren, A., Giardino, A., Vousdoukas, M., Gaytan-Aguilar, S. and Ranasinghe, R.: Global distribution of nearshore slopes with implications for coastal retreat, Earth Syst. Sci. Data Discuss., 11(4), 1–29, doi:10.5194/essd-2019-71, 2019.

Aucan, J., Hoeke, R. K., Storlazzi, C. D., Stopa, J., Wandres, M. and Lowe, R.: Waves do not contribute to global sea-level
315   rise, Nat. Clim. Chang., 9(1), 2–2, doi:10.1038/s41558-018-0377-5, 2019.

Bishop-Taylor, R., Sagar, S., Lymburner, L. and Beaman, R. J.: Between the tides: Modelling the elevation of Australia's exposed intertidal zone at continental scale, Estuar. Coast. Shelf Sci., 223(October 2018), 115–128, doi:10.1016/j.ecss.2019.03.006, 2019.

Bujan, N., Cox, R. and Masselink, G.: From fine sand to boulders: examining the relationship between beach-face slope and
320   sediment size., Mar. Geol., 106012, doi:10.1016/j.margeo.2019.106012, 2019.

Carrere, L., Lyard, F., Cancet, M., Guillot, A. and Picot, N.: FES 2014, a new tidal model—Validation results and perspectives for improvements, in Proceedings of the ESA living planet symposium, pp. 9–13., 2016.

Coastal Engineering Research Center: Shore protection manual, Dept. of the Army, Waterways Experiment Station, Corps of

325   Engineers, Coastal Engineering Research Center. [online] Available from: https://books.google.com.au/books?id=km0YAQAAIAAJ, 1984.

Dean, R. G. and Dalrymple, R. A.: Coastal processes with engineering applications, Cambridge University Press., 2004.

Eleveld, M. A., Van der Wal, D. and Van Kessel, T.: Estuarine suspended particulate matter concentrations from sun-synchronous satellite remote sensing: Tidal and meteorological effects and biases, Remote Sens. Environ., 143, 204–215, doi:10.1016/j.rse.2013.12.019, 2014.

330   Gomes da Silva, P., Coco, G., Garnier, R. and Klein, A. H. F.: On the prediction of runup, setup and swash on beaches, Earth-Science Rev., 204, 103148, doi:10.1016/J.EARSCIREV.2020.103148, 2020.

Gopalakrishnan, S., Smith, M. D., Slott, J. M. and Murray, A. B.: The value of disappearing beaches: A hedonic pricing model with endogenous beach width, J. Environ. Econ. Manage., 61(3), 297–310, doi:10.1016/J.JEEM.2010.09.003, 2011.

GRASS Development Team: Geographic Resources Analysis Support System (GRASS GIS) Software, [online] Available
335   from: https://grass.osgeo.org, 2020.

Greenslade, D., Hemer, M., Babanin, A., Lowe, R., Turner, I., Power, H., Young, I., Ierodiaconou, D., Hibbert, G., Williams, G., Aijaz, S., Albuquerque, J., Allen, S., Banner, M., Branson, P., Buchan, S., Burton, A., Bye, J., Cartwright, N., Chabchoub, A., Colberg, F., Contardo, S., Dufois, F., Earl-Spurr, C., Farr, D., Goodwin, I., Gunson, J., Hansen, J., Hanslow, D., Harley, M., Hetzel, Y., Hoeke, R., Jones, N., Kinsela, M., Liu, Q., Makarynskyy, O., Marcollo, H., Mazaheri, S., McConochie, J.,
340   Millar, G., Moltmann, T., Moodie, N., Morim, J., Morison, R., Orszaghova, J., Pattiaratchi, C., Pomeroy, A., Proctor, R., Provis, D., Reef, R., Rijnsdorp, D., Rutherford, M., Schulz, E., Shayer, J., Splinter, K., Steinberg, C., Strauss, D., Stuart, G., Symonds, G., Tarbath, K., Taylor, D., Taylor, J., Thotagamuwage, D., Toffoli, A., Valizadeh, A., Van Hazel, J., Da Silva, G. V., Wandres, M., Whittaker, C., Williams, D., Winter, G., Xu, J., Zhong, A. and Zieger, S.: 15 priorities for wind-waves research: An Australian perspective, Bull. Am. Meteorol. Soc., 101(4), E446–E461, doi:10.1175/BAMS-D-18-0262.1, 2020.

345   Leaman, C. K., Harley, M. D., Splinter, K. D., Thran, M. C., Kinsela, M. A. and Turner, I. L.: A storm hazard matrix combining coastal flooding and beach erosion, Coast. Eng., 170, 104001, doi:10.1016/J.COASTALENG.2021.104001, 2021.

Melet, A., Meyssignac, B., Almar, R. and Le Cozannet, G.: Under-estimated wave contribution to coastal sea-level rise, Nat. Clim. Chang., 8(3), 234–239, doi:10.1038/s41558-018-0088-y, 2018.

Middleton, J. H., Cooke, C. G., Kearney, E. T., Mumford, P. J., Mole, M. A., Nippard, G. J., Rizos, C., Splinter, K. D. and
350   Turner, I. L.: Resolution and accuracy of an airborne scanning laser system for beach surveys, J. Atmos. Ocean. Technol., 30(10), 2452–2464, doi:10.1175/JTECH-D-12-00174.1, 2013.

O'Grady, J. G., McInnes, K. L., Hemer, M. A., Hoeke, R. K., Stephenson, A. G. and Colberg, F.: Extreme Water Levels for Australian Beaches Using Empirical Equations for Shoreline Wave Setup, J. Geophys. Res. Ocean., 124(8), 5468–5484, doi:10.1029/2018jc014871, 2019.

355   OSM: OpenStreetMap contributers: Planet dump retrieved from https://planet.osm.org, 2017.

Phillips, M. R. and House, C.: An evaluation of priorities for beach tourism: Case studies from South Wales, UK, Tour.

Manag., 30(2), 176–183, doi:10.1016/J.TOURMAN.2008.05.012, 2009.

Power, H. E., Pomeroy, A. W. M., Kinsela, M. A. and Murray, T. P.: Research Priorities for Coastal Geoscience and Engineering: A Collaborative Exercise in Priority Setting From Australia, Front. Mar. Sci., 8, 252,

360   doi:10.3389/fmars.2021.645797, 2021.

Pucino, N.: Coastal Dune Morphodynamic and Measures for Sand Stabilisation in Stockton Bight (NSW), University of Wollongong., 2015.

Pucino, N., Kennedy, D. M., Carvalho, R. C., Allan, B. and Ierodiaconou, D.: Citizen science for monitoring seasonal-scale beach erosion and behaviour with aerial drones, Sci. Reports 2021 111, 11(1), 1–17, doi:10.1038/s41598-021-83477-6, 2021.

365   QGIS Development Team: QGIS Geographic Information System, [online] Available from: https://www.qgis.org, 2021.

Senechal, N., Coco, G., Bryan, K. R. and Holman, R. A.: Wave runup during extreme storm conditions, J. Geophys. Res. Ocean., 116(7), C07032, doi:10.1029/2010JC006819, 2011.

Short, A. D.: Australian Coastal Systems, vol. 32, Springer International Publishing, Cham., 2020.

Short, A. D., Williamson, B. and Hogan, C. L.: The Australian Beach Safety and Management Program - Surf Life Saving

370   Australia's Approach to Beach Safety and Coastal Planning, 11th Australas. Conf. Coast. Ocean Eng. (Townsville, Qld.), National   c(93/4),   113–118   [online]   Available   from: https://search.informit.com.au/documentSummary;dn=560087890263399;res=IELENG, 1993.

Small, C., Nicholls, R. J., Summer, F. and Smallt, C.: A Global Analysis of Human Settlement in Coastal Zones, J. Coast. Res., 19(3), 584–599, doi:10.2307/4299200, 2011.

375   Stephens, S. A., Coco, G. and Bryan, K. R.: Numerical Simulations of Wave Setup over Barred Beach Profiles: Implications for Predictability, J. Waterw. Port, Coast. Ocean Eng., 137(4), 175–181, doi:10.1061/(ASCE)WW.1943-5460.0000076, 2011.

Stockdon, H. F., Asbury H., Jr., S., List, J. H. and Holman, R. A.: Estimation of Shoreline Position and Change Using Airborne Topographic Lidar Data, J. Coast. Res., 18(3), 502–513, doi:10.2307/4299097, 2002.

Stockdon, H. F., Holman, R. A., Howd, P. A. and Sallenger, A. H.: Empirical parameterization of setup, swash, and runup,

380   Coast. Eng., 53(7), 573–588, doi:10.1016/j.coastaleng.2005.12.005, 2006.

Stockdon, H. F., Sallenger, A. H., Holman, R. A. and Howd, P. A.: A simple model for the spatially-variable coastal response to hurricanes, Mar. Geol., 238(14), 1–20, doi:10.1016/j.margeo.2006.11.004, 2007.

Stokes, K., Poate, T. and Masselink, G.: Development of a real-time, regional coastal flood warning system for southwest England, in Coastal Sediments 2019, pp. 1460–1474, World Scientific Pub Co Pte Lt., 2019.

385   Thom, B. G., Eliot, I., Eliot, M., Harvey, N., Rissik, D., Sharples, C., Short, A. D. and Woodroffe, C. D.: National sediment compartment framework for Australian coastal management, Ocean Coast. Manag., 154(July 2017), 103–120, doi:10.1016/j.ocecoaman.2018.01.001, 2018.

Tseng, K. H., Kuo, C. Y., Lin, T. H., Huang, Z. C., Lin, Y. C., Liao, W. H. and Chen, C. F.: Reconstruction of time-varying tidal flat topography using optical remote sensing imageries, ISPRS J. Photogramm. Remote Sens., 131, 92–103,

390   doi:10.1016/j.isprsjprs.2017.07.008, 2017.

Turner, I. L., Harley, M. D. and Drummond, C. D.: UAVs for coastal surveying, Coast. Eng., 114, 19–24, doi:10.1016/j.coastaleng.2016.03.011, 2016.

VanderPlas, J. T.: Understanding the Lomb–Scargle Periodogram, Astrophys. J. Suppl. Ser., 236(1), 16, doi:10.3847/1538-4365/aab766, 2018.

395   Vitousek, S., Barnard, P. L., Fletcher, C. H., Frazer, N., Erikson, L. and Storlazzi, C. D.: Doubling of coastal flooding frequency within decades due to sea-level rise, Sci. Rep., 7(1), 1–9, doi:10.1038/s41598-017-01362-7, 2017.

Vos, K.: kvos/CoastSat: CoastSat v1.1.1, , doi:10.5281/ZENODO.4649450, 2021a.

Vos, K.: kvos/CoastSat.slope: CoastSat.slope v1.0.2, , doi:10.5281/ZENODO.5372830, 2021b.

Vos, K., Splinter, K. D., Harley, M. D., Simmons, J. A. and Turner, I. L.: CoastSat: A Google Earth Engine-enabled Python
400   toolkit to extract shorelines from publicly available satellite imagery, Environ. Model. Softw., 122, 104528, doi:10.1016/j.envsoft.2019.104528, 2019a.

Vos, K., Harley, M. D., Splinter, K. D., Simmons, J. A. and Turner, I. L.: Sub-annual to multi-decadal shoreline variability from publicly available satellite imagery, Coast. Eng., 150, 160–174, doi:10.1016/j.coastaleng.2019.04.004, 2019b.

Vos, K., Harley, M. D., Splinter, K. D., Walker, A. and Turner, I. L.: Beach Slopes From Satellite-Derived Shorelines,
405   Geophys. Res. Lett., 47(14), doi:10.1029/2020GL088365, 2020.

Vos, K., Harley, M. D., Splinter, K. D., Turner, I. L. and Wen, D.: Beach-face slope dataset for Australia, , doi:10.5281/ZENODO.5606217, 2021.

Wright, L. D. and Short, A. D.: Morphodynamic variability of surf zones and beaches: A synthesis, Mar. Geol., 56(1–4), 93–118, doi:10.1016/0025-3227(84)90008-2, 1984.

410